A NEW SUBMESH STRATEGY IN THE TWO-LEVEL FINITE ELEMENT METHOD FOR THE ADVECTIVE-DIFFUSIVE EQUATION

by

Feng-Nan Hwang

B.S., Fu-Jen Catholic University, Taiwan, 1995

A thesis submitted to the

University of Colorado at Denver

in partial fulfillment

of the requirements for the degree of

Master of Science

Applied Mathematics

1999

This thesis for the Master of Science

degree by

Feng-Nan Hwang

has been approved

by

Leopoldo P. Franca

Thomas Russell

Andrew Knyazev

Date

Hwang, Feng-Nan (M.S., Applied Mathematics)

A New Submesh Strategy in the Two-Level Finite Element Method for the Advective-Diffusive Equation

Thesis directed by Professor Leopoldo P. Franca

ABSTRACT

The residual-free bubble (RFB) method for the general boundary value problem is reviewed. The two level finite element method (TLFEM) derived from the RFB method and its application to the advective-diffusive equation are addressed. There is a boundary layer near outflow boundaries for the bubble shape functions when the flow is advective dominated. In this work, we introduce a new submesh strategy depending on the direction of the flow in the TLFEM and design an algorithm for generating this submesh. The numerical results show that the new submesh is able to capture the boundary layer which is caused by the choice of bubble functions. The effect of a more accurately approximated residual free bubble function produces some improvements in the solution of the advective-diffusive equation.

This abstract accurately represents the content of the candidate's thesis. I recommend its publication.

Signed _____

Leopoldo P. Franca

DEDICATION

To my parents and Tzu-Chia

ACKNOWLEDGMENTS

First, I would like thank my advisor, Professor Leo Franca, for his instructive guidance and wonderful patience during the preparation of this thesis. Also thanks to the members of our research group, especially Ali Nesliturk and Saulo P. Oliveira, for their technical support on programming. Finally, thanks goes to Randy Chase for his linguistic assistance.

CONTENTS

FIGURES

Figure

1. Introduction

We approximate the advective-diffusive equation in this work. There are a lot of applications in fluid dynamics using this model as well as in the semiconductor industry. For the advective-diffusive equation, the behavior of the solution depends on the magnitude of the velocity field and the diffusivity coefficient.

Let us define the mesh-Peclet number as $Pe = \frac{|\boldsymbol{a}|h}{2\kappa}$. Here, $\boldsymbol{a}$ is the velocity field, h is the mesh size and κ is the diffusivity coefficient. When this number is large, we say the model is advective dominated; otherwise, it is diffusive dominated. In the finite element literature, it is well known that the standard Galerkin method using piecewise linears performs poorly for the advective dominated model. Spurious oscillations are frequently detected in the solution.

In order to overcome this difficulty, stabilized finite element methods have been introduced [3, 5, 10], and one version was denoted by the Galerkin least-squares method (GLS). The GLS method adds an 'artificial' term to the variational formulation. This additional term not only improves the numerical stability of the Galerkin method but also preserves good accuracy.

On the other hand, it is not hopeless to apply the standard Galerkin method to solve this problem. Herein we are interested in approximating the residual-free bubble (RFB) method using the Galerkin method. The bubble function is chosen so that the computed solution satisfies the original differential equation in the interior of each element and vanishes on the boundary of each element.

In [1] a relationship is established between the stabilized finite element method and the Galerkin method using piecewise linears enriched with one bubble per element for the advective-diffusive model. Therein these two methods are shown to be equivalent for diffusive dominated models and appropriately defined element parameters h_k. Later Brezzi, Franca and Russo [2] proved the coercivity /stability inequality for a limiting case of the RFB method. Further progress has been made by Franca, Nesliturk and Stynes in [7], where they obtained the desired stability condition for positive but small diffusivity parameters under some hypotheses that the flow velocity is constant, the triangulation is regular, and the edges of triangulation are bounded away from the direction of flow.

A challenge for the RFB method is to determine the residual free bubble functions in a higher dimensional situation. The two-level finite element method (TLFEM) is a general framework to resolve this task. This method

was first successfully used for solving the Helmholtz equation [6]. In [7], the numerical results for the advection-diffusion problem showed that the TLFEM performed as well as GLS and that there is no major qualitative difference between these two methods. The TLFEM consists in partitioning the mesh into submeshes, and an appropriate numerical method is then used to approximate the PDE's governing the residual-free bubble basis functions instead of solving analytically for the residual-free bubble functions. We can partition each mesh into different submeshes arbitrarily. For simplicity of implementation, uniform submeshes are considered first. However, due to the choice of bubble functions, there might be boundary layers near outflow boundaries for the bubble shape functions. Therefore, it seems more appropriate to choose a new submesh which is able to capture the layer to produce more accurate approximate residual-free bubble shape functions.

The purpose of this thesis is to introduce the new nonuniform submeshes depending on the direction of the flow, and compare numerical solutions of the TLFEM for advection-diffusion with uniform submeshes to see if we can get any improvement on the numerical solutions under the same global mesh.

This thesis is organized as follows: In the next chapter, we review the residual-free bubble method for the general boundary value problem. Then,

in chapter 3, we discuss the two-level finite element method for the advective-diffusive equation derived from the RFB method ; In chapter 4, the algorithm for generating non-uniform submesh is developed. Finally, numerical results and conclusions are presented in chapter 5 and chapter 6 respectively.

2. The review of RFB for boundary value problems

Let us consider Ω to be an open bounded domain in R^2 with boundary $\partial\Omega$. For simplicity, we assume that $\partial\Omega$ is a polynomial curve in which case we say that Ω is a polynomial domain. (If $\partial\Omega$ is a curve, we can approximate it with a polynomial).

First, we consider the general boundary value problem

$$\begin{cases} Lu = f & \text{in} \quad \Omega \\ u = 0 & \text{on} \quad \partial\Omega \end{cases} \tag{2.1}$$

where L is a linear differential operator, e.g. L may be the advective-diffusive operator, u is the unknown scalar function and f is a given source function. We also assume that this problem is well posed.

The abstract variational formulation of (2.1) is as follows: Find a scalar variable $u \in V$ such that

$$a(u, v) = (f, v) \qquad \forall \ v \in V, \tag{2.2}$$

where V is a Hilbert space, $a(\cdot, \cdot)$ is a bilinear form from $V \times V$ to R and $(\cdot, \cdot)$ is the usual scalar product in $L^2(\Omega)$.

To specify the standard Galerkin finite element for (2.1), we partition the

domain Ω into several pieces K (e.g. triangles, quadrilaterals etc.) in the standard way, which forbids overlapping or any vertex on the edge of a neighboring element, and so on. Thus,

$$\Omega = \bigcup_{K \in T_h} K = K_1 \cup K_2 \cup \ldots \cup K_m \tag{2.3}$$

where T_h is a partition of Ω.

We introduce the mesh parameter

$$h = \max_{K \in T_h} \text{diam}(K), \text{ diam}(K) = \text{ diameter of } K \tag{2.4}$$

We now define V_h as a finite-dimensional space, which is a subspace of V. Then the standard Galerkin finite element method is: Find $u_h \in V_h$ such that

$$a(u_h, v_h) = (f, v_h) \qquad \forall \ v_h \in V_h \tag{2.5}$$

Now, we decompose the space V_h such that $V_h = V_1 + B$, where V_1 is the space of continuous piecewise linear or bilinear polynomials and B is the space of residual-free bubbles . We will define the space B explicitly later. Then every $u_h \in V_h$ can be written in the form of $u_h = u_1 + u_b$, where $u_1 \in V_1$ and $u_b \in B$. For the residual-free bubble space, we require the bubble component u_b of each v_h to vanish on ∂K of each K and require each v_h to satisfy the original differential equations strongly, i.e.

$$L(u_1 + u_b) = f \qquad \text{in} \quad K \tag{2.6}$$

$$\text{or} \qquad Lu_b = -(Lu_1 - f) \qquad \text{in} \quad K \tag{2.7}$$

subject to zero Dirichlet boundary condition on the element boundary, i.e.

$$u_b = 0 \quad \text{on} \quad \partial K. \tag{2.8}$$

By the classical static condensation procedure, first we set $v_h = v_{b,K}$ in K and $v_h = 0$ elsewhere in (2.5) to have

$$a(u_1 + u_b, v_{b,K})_K = (f, v_{b,K})_K \qquad \forall v_{b,K} \in B \tag{2.9}$$

where $a(\cdot,\cdot)_K$ and $(\cdot,\cdot)_K$ indicate that integration is restricted to the element K.

Then, taking $v_h = v_1$ in (2.5), we obtain

$$a(u_h, v_1) = (f, v_1) \tag{2.10}$$

$$\text{or} \quad a(u_1 + u_b, v_1) = (f, v_1) \tag{2.11}$$

The formulation (2.9) is automatically true due to our choice of bubble functions. In fact, this equation is also the variational formulation of (2.6) using v_b as test function restricted to each element K. Furthermore, the equation (2.11) is the method to compute an improved bilinear or linear approximation due to the residual-free bubbles effect. To find the residual-free bubble part of the solution, we need to solve (2.5) which depends on the linear part of the

solution u_1. Instead, bubble shape functions with i varying from one to the number of element nodes (Nen) can be obtained by the following auxiliary problems:

(i) For each i=1, 2, ... Nen, find $\phi_{i,K}$ such that

$$L\phi_{i,K} = -L\psi_{i,K} \quad \text{in} \quad K \tag{2.12}$$

$$\phi_{i,K} = 0 \quad \text{on} \quad \partial K \tag{2.13}$$

where the $\psi_{i,K}$ are local basis function for u_1 and

(ii) find $\phi_{f,K}$ such that

$$L\phi_{f,K} = f \quad \text{in} \quad K \tag{2.14}$$

$$\phi_{f,K} = 0 \quad \text{on} \quad \partial K \tag{2.15}$$

Thus if

$$u_1 = \sum_{i=1}^{Nen} c_{i,K}\phi_{i,K} \tag{2.16}$$

then

$$u_b = \sum_{i=1}^{Nen} c_{i,K}\psi_{i,K} + \psi_{f,K} \tag{2.17}$$

with the same coefficient $c_{i,K}$.

Furthermore, we have the following representation:

$$u_{h,K} = \sum_{i=1}^{Nen} c_{i,K}(\psi_{i,K} + \phi_{i,K}) + \phi_{f,K}. \tag{2.18}$$

Hence, we can define the residual-free bubble space B_K as

$$B_K = span\{\phi_{1,K}, \ldots, \phi_{Nen,K}, \phi_f\} \tag{2.19}$$

and

$$B = \sum_{K \in T_h} B_K \tag{2.20}$$

Therefore, we can restate the RFB method for general boundary value problem as the following:

$$\begin{cases} \text{Find} \quad u_h = u_1 + u_b \in V_h = V_1 + B \quad \text{such that} \\ \quad a(u_h, v_1) = (f, v_1) \qquad\qquad \forall v_1 \in V_1 \\ a(u_h, v_{b,K})_K = (f, v_{b,K})_K \qquad \forall K \in T_h \qquad \text{and} \qquad v_{b,K} \in B_K \end{cases} \tag{2.21}$$

or we can eliminate $u_{b,K}$ in (2.21) and obtain an equation which only involves u_1:

$$\begin{cases} \text{Find} \quad u_1 \in V_1 \quad \text{such that} \\ \qquad a(u_1, v_1) + \sum_{K \in T_h} a(u_{b,K}, v_1)_K = (f, v_1) \quad \forall v_1 \in V_1 \end{cases} \tag{2.22}$$

To get $u_{b,K}$ as a function of u_1 and f requires solving equations (2.12)-(2.15), which is as complicated as solving the original differential equation, unless we have special cases such as rectangular elements such that we can employ classical analytical tools to get an exact solution within each element. Henceforth our strategy is to approximate the bubble shape functions $\psi_{i,K}$ and $\psi_{f,K}$ by another appropriate finite element method. In other words, at the global level we

use the standard Galerkin method with piecewise linears for the original problem. At the element level, we partition each element into a finer submesh and then utilize non-standard finite element methods to solve the bubble problems. This is why we called this method a two-level finite element method (TLFEM). In this work, instead of GLS, we apply the improved Unusual Stabilized Finite Element Method (the improved US-FEM) [8] to approximate the bubble shape functions. We discuss TLFEM in more detail in the next section.

3. The TLFEM for the advective-diffusive problem

In the present section we develop the TLFEM based on the RFB method and discuss its application to the advective-diffusive problem. This approach is general, and can be applied to an arbitrarily shaped domain without any difficulty. For the advective-diffusive problem, we set

$$L = -\kappa\triangle + \boldsymbol{a}\cdot\nabla \tag{3.1}$$

Here $\boldsymbol{a}$ is the given velocity field, assumed to be constant in each element, and κ is the given positive constant diffusivity coefficient. We are interested in the advective-dominated case, i.e. when $\kappa \ll |\boldsymbol{a}|$. The associated bilinear form is

$$a(u,v) = \kappa(\nabla u, \nabla v) + (\boldsymbol{a}\cdot\nabla u, v) \tag{3.2}$$

At the global level, we rewrite equation (2.11) for the advective-diffusive problem:

$$\kappa(\nabla u_1, \nabla v_1) + \kappa(\nabla u_b, \nabla v_1) + (\boldsymbol{a}\cdot\nabla u_1, v_1) + (\boldsymbol{a}\cdot\nabla u_b, v_1) = (f, v_1) \tag{3.3}$$

Then, let us consider the second term above:

$$\begin{aligned}\kappa(\nabla u_b, \nabla v_1) &= \sum_K \kappa(\nabla u_b, \nabla v_1)_K \\ &= \sum_K \kappa \int_K \nabla u_b \cdot \nabla v_1 \, dx \\ &= \sum_K (\kappa \int_{\partial K} u_b \nabla v_1 \cdot \boldsymbol{n} \, ds - \kappa \int_K u_b \triangle v_1 \, dx),\end{aligned}$$

where $\boldsymbol{n}$ is an unit normal vector. The last equality is obtained by integration-by-parts. Since the residual-free bubble function u_b's are zero on element boundaries and v_1 is bilinear inside rectangular elements, we conclude that $\kappa(\nabla u_b, \nabla v_1) = 0$.

Therefore, equation (3.3) simplifies to

$$\kappa(\nabla u_1, \nabla v_1) + (\boldsymbol{a} \nabla u_1, v_1) + (\boldsymbol{a} \cdot \nabla u_b, v_1) = (f, v_1) \tag{3.4}$$

Substituting (2.18) into (3.4) and setting $v_1 = \psi_j$ enables us to write the matrix problem: Find the coefficient c_i's such that

$$\sum_i c_i[(\kappa \nabla \psi_i, \nabla \psi_j) + (\boldsymbol{a} \cdot \nabla \psi_i, \psi_j) + (\boldsymbol{a} \cdot \nabla \phi_i, \psi_j)] = (f, \psi_j) - (\boldsymbol{a} \cdot \nabla \phi_f, \psi_j) \tag{3.5}$$

i runs over all unknown interior nodes in the elements, say through N.

At the local element level, (2.12)-(2.15) for the advective-diffusive problem reads:

(i) for $i = 1, \cdots, Nen$,

$$\boldsymbol{a} \cdot \nabla \phi_{i,K} - \kappa \triangle \phi_{i,K} = -\boldsymbol{a} \cdot \nabla \psi_{i,K} \quad \text{in} \quad K \tag{3.6}$$

$$\phi_{i,K} = 0 \quad \text{on} \quad \partial K \tag{3.7}$$

(ii)

$$\boldsymbol{a} \cdot \nabla \phi_{f,K} - \kappa \triangle \phi_{f,K} = f \quad \text{in} \quad K \tag{3.8}$$

$$\phi_{f,K} = 0 \quad \text{on} \quad \partial K \tag{3.9}$$

For each element K, let $\partial K^- = \{ \boldsymbol{x} \in \partial K : \boldsymbol{a} \cdot \boldsymbol{n}(\boldsymbol{x}) < 0\}$ be its inflow boundary and $\partial K^+ = \{ \boldsymbol{x} \in \partial K : \boldsymbol{a} \cdot \boldsymbol{n}(\boldsymbol{x}) \geq 0\}$ be its outflow boundary, where $\boldsymbol{n}$ is the outward normal unit vector to ∂K. Assume that $\boldsymbol{a} \cdot \boldsymbol{n}(\boldsymbol{x})$ is bounded away from zero; then we have $\partial K = \partial K^- \bigcup \partial K^+$.

For small diffusivity we wish to consider the corresponding reduced problems obtained by setting κ =0:

(i) for $i = 1, \cdots, Nen$,

$$\boldsymbol{a} \cdot \nabla \phi_{i,K} = -\boldsymbol{a} \cdot \nabla \psi_{i,K} \quad \text{in} \quad K \tag{3.10}$$

$$\phi_{i,K} = 0 \quad \text{on} \quad \partial K^- \tag{3.11}$$

(ii)

$$\boldsymbol{a} \cdot \nabla \phi_{f,K} = f \qquad \text{in} \quad K \tag{3.12}$$

$$\phi_{f,K} = 0 \qquad \text{on} \quad \partial K^- \tag{3.13}$$

The characteristics of the reduced problems (3.10) and (3.12) are straight lines parallel to the velocity field $\boldsymbol{a}$.

Let us state some basic facts concerning the exact solutions of (3.6), (3.7), (3.8) and (3.9):

(i) If we consider that the inflow boundary data of the reduced problem is a discontinuous function g instead of the zero function, then the solution of the reduced problem may be discontinuous with a jump across the characteristic. In the full problem, the solution is continuous in K and the jump will be spread out in a small region around the characteristic.

(ii) If the values attained by the reduced problems on ∂K^+ do not coincide with the boundary values described in the full problems, then solutions of the latter problems will have a boundary layer at ∂K^+; i.e. at a very narrow region near the outflow boundary of the element, where the solution and its derivative change abruptly.

For a given unit vector $\boldsymbol{v}$ with components (v_1, v_2), the directional derivative

of u is defined by

$$\boldsymbol{v}\cdot\nabla u = D_{\boldsymbol{v}} u \tag{3.14}$$

In other word, $D_v u$ is the component of ∇u is the direction of $\boldsymbol{v}$. Hence, $\boldsymbol{a}\cdot\nabla\phi_{i,K}$ can be viewed as the directional derivative of $\phi_{i,K}$ in the streamline direction multiplied by $|\boldsymbol{a}|$, similarly for $\boldsymbol{a}\cdot\nabla\psi_{i,K}$ and $\boldsymbol{a}\cdot\nabla\phi_{f,K}$. Therefore, the analytical solution of (3.10) and (3.11) can be obtained simply by taking integrals from $\boldsymbol{x}^-$ to $\boldsymbol{x}$ at both sides of the equations along the streamline direction and then applying the fundamental theorem of calculus. The solution of (3.10) and (3.11) is given by:

$$\phi_{i,K}(\boldsymbol{x}) = -\psi_{i,K}(\boldsymbol{x}) + \psi_{i,K}(\boldsymbol{x}^-) \tag{3.15}$$

and similarly the solution of (3.12) and (3.13) is:

$$\phi_{f,K}(\boldsymbol{x}) = \frac{1}{|\boldsymbol{a}|}\int_{\boldsymbol{x}^-}^{\boldsymbol{x}} f\, ds \tag{3.16}$$

where $\boldsymbol{x}^-$ is the intersection of a line parallel to $\boldsymbol{a}$ passing through the point $\boldsymbol{x}$ in (3.15) with the inflow boundary ∂K^-. In addition, we define $\boldsymbol{x}^+$ as the

coordinate of the point on the outflow boundary ∂K^+, aligned with the point $\boldsymbol{x}^+$ in the streamline direction. (See Figure 3.1)

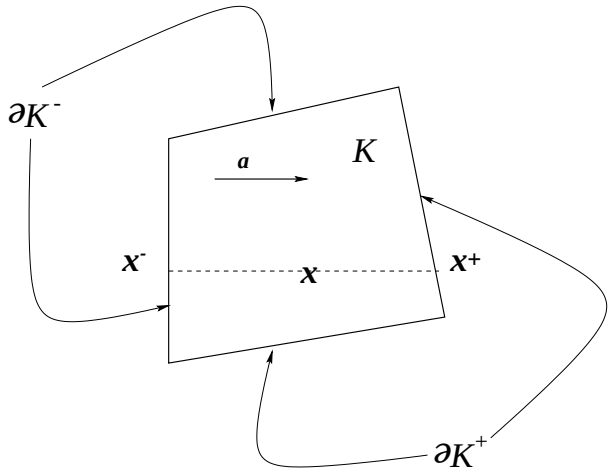

Figure 3.1. Obtaining $\boldsymbol{x}^-$ and $\boldsymbol{x}^+$ from any $\boldsymbol{x} \in K$

To get the general idea of the behavior of the residual-free bubble shape function, let us consider a simple example:

Let K be an unit square element defined in [0,1]$\times$ [0,1] with an uniform velocity field of size one forming a 45^o with the horizontal axis. (See Figure 3.2)

We assume the nodal points are labeled in ascending order in the counterclockwise direction and let Side(1) be the edge joining the nodal points 1 and 2, the Side(2) is the edge joining the nodal point 2 and 3 and so on. (See Figue 3.3).

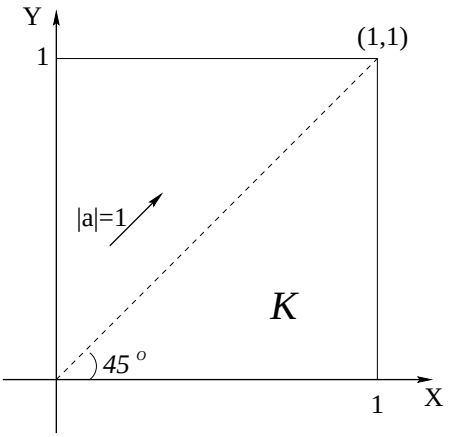

Figure 3.2. Problem statement

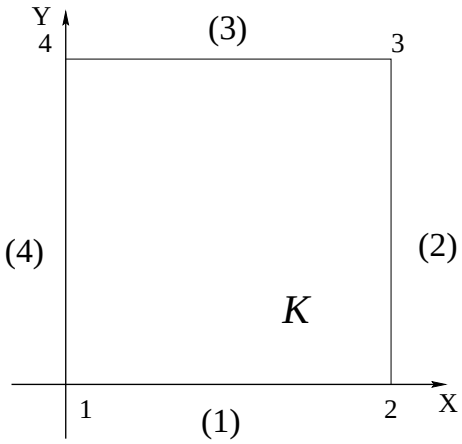

Figure 3.3. Nodal points and sides numbering

It can be easily seen that Side(1) and Side(4) are inflow boundaries and Side(2) and Side(3) are outflow boundaries for this example. Then, we can define the local shape function $\psi_i(x)$'s explicitly.

$$\begin{aligned}
\psi_1(x,y) &= (1-x)(1-y) \\
\psi_2(x,y) &= x(1-y) \\
\psi_3(x,y) &= xy \\
\psi_4(x,y) &= (1-x)y
\end{aligned}$$

By formula (3.15), the values of each bubble shape function on the outflow boundary ∂K^+ can be evaluated by:

$$\begin{aligned}
\phi_1(x,y) &= \begin{cases} 1-x & : \text{ on Side(2)} \\ 1-y & : \text{ on Side(3)} \end{cases} \\
\phi_2(x,y) &= 0 \\
\phi_3(x,y) &= \begin{cases} -y & : \text{ on Side(2)} \\ -x & : \text{ on Side(3)} \end{cases} \\
\phi_4(x,y) &= 0
\end{aligned}$$

For bubble functions ϕ_1 and ϕ_3, the values on ∂K^+ are different from the

boundary values prescribed in the full problems. It turns out that we are expecting there may be an outflow boundary layer for these bubble shape functions. This example gives us a general idea of how to choose the optimal submesh (a mesh defined for each element) which is able to capture a jump discontinuity of the exact solution in a thin numerical layer. Our strategy is to use the nonuniform submesh which is more refined near the outflow boundaries depending on the direction of the velocity field. Figure 3.4 illustrates this idea.

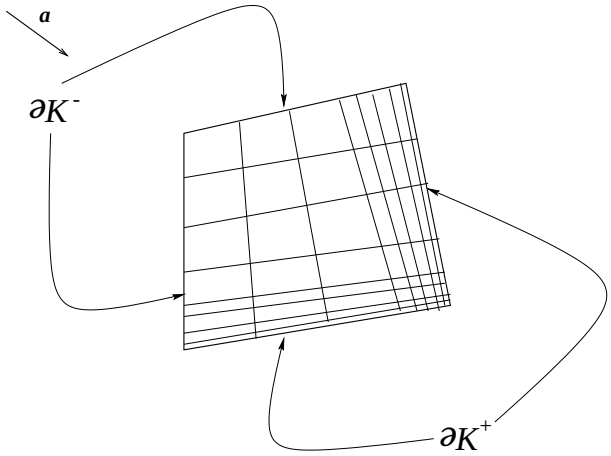

Figure 3.4. Submesh refines on outflow boundaries

We begin to approximate residual-free bubble shape functions by partitioning each element K into the coarse submesh K^* (a mesh defined for each element) with diameter h^* and denote by ψ_l^* the basis function for a piecewise linear interpolation on the submesh.

Therefore, our unknown bubble basis function can be approximated by

$$\phi_i^{h^*} = \sum_l^{N^*} c_l^{(i)} \psi_l^* \tag{3.17}$$

Here N^* is the number of all unknown interior node in the submesh. The index i refers to specific bubble function that we are trying to compute.

Similarly, under the presence of a source term f, the other bubble shape function is given by:

$$\phi_f^{h^*} = \sum_l^{N^*} c_l^f \psi_l^* \tag{3.18}$$

Then we can formulate the improved US-FEM [8] for the case in which the reactive term is equal to zero in the matrix formulation for (3.6) and (3.7) as: for each i (from 1 to Nen) find $c_l^{(i)}$, such that

$$\sum_l c_l^{(i)} [(\boldsymbol{a} \cdot \nabla \psi_l^*, \psi_m^*) + (\kappa \nabla \psi_l^*, \nabla \psi_m^*) + (\boldsymbol{a} \cdot \nabla \psi_l^*, \tau a \cdot \psi_m^*)]$$
$$= (-\boldsymbol{a} \cdot \nabla \psi_{i,K}, \psi_m^* + \tau \boldsymbol{a} \cdot \nabla \psi_m^*) \tag{3.19}$$

In addition, the matrix formulation for (3.8)-(3.9) is given by: find c_l^f, such that

$$\sum_l c_l^f [(\boldsymbol{a} \cdot \nabla \psi_l^*, \psi_m^*) + (\kappa \nabla \psi_l^*, \nabla \psi_m^*) + (\boldsymbol{a} \cdot \nabla \psi_l^*, \tau \boldsymbol{a} \cdot \psi_m^*)] = (f, \psi_m^* + \tau \boldsymbol{a} \cdot \nabla \psi_m^*) \tag{3.20}$$

We use the stability τ suggested in [8] as

$$\tau(x, Pe_K(x)) \quad = \quad \frac{{h_K^*}^2}{6\kappa + 6\kappa \xi(Pe_K(x))}, \tag{3.21}$$

$$Pe_K(x) = \frac{|\boldsymbol{a}(x)|_2 h^*{}_K}{3\kappa(x)}, \tag{3.22}$$

$$\xi(x) = \begin{cases} 1 \quad , & \text{if } 0 \le x < 1, \\ x \quad , & \text{if } x \ge 1, \end{cases} \tag{3.23}$$

$$|\boldsymbol{a}(x)|_2 = \sum_{i=1}^{2} (|a_i(x)^2|)^{1/2}. \tag{3.24}$$

And the element parameter h_K^* is computed by using the largest streamline distance of elements. See Figure 3.5.

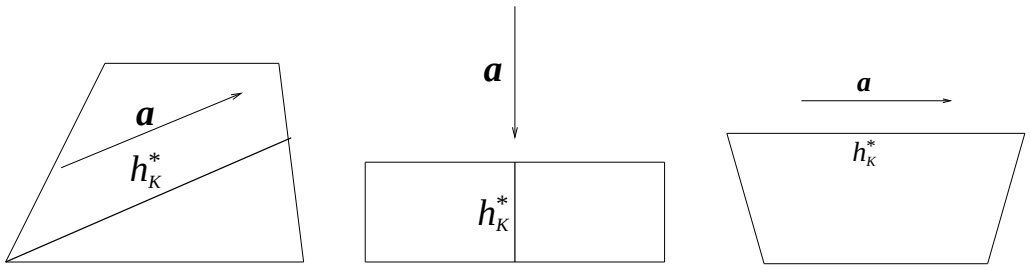

Figure 3.5. The element parameter computation

Once the constants $c_l^{(i)}$ and c_l^f are determined, we substitute them in (3.17) and (3.18) respectively to get the approximate residual basis function $\psi_i^{h^*}$ and $\psi_f^{h^*}$.

For a practical problem such as the flow over an airfoil or an automobile, the direction of the flow varies element-wise. Therefore, it is necessary for us to design a subroutine in our computer program to generate the non-uniform submesh automatically. Before proceeding to discuss the algorithm for a submesh

generator, let us list all combinations of outflow and inflow boundary segments of elements and indicate the submeshes which are used for each different case. Other permutations are not listed, since they are covered by all combinations listed in Figure 3.6.

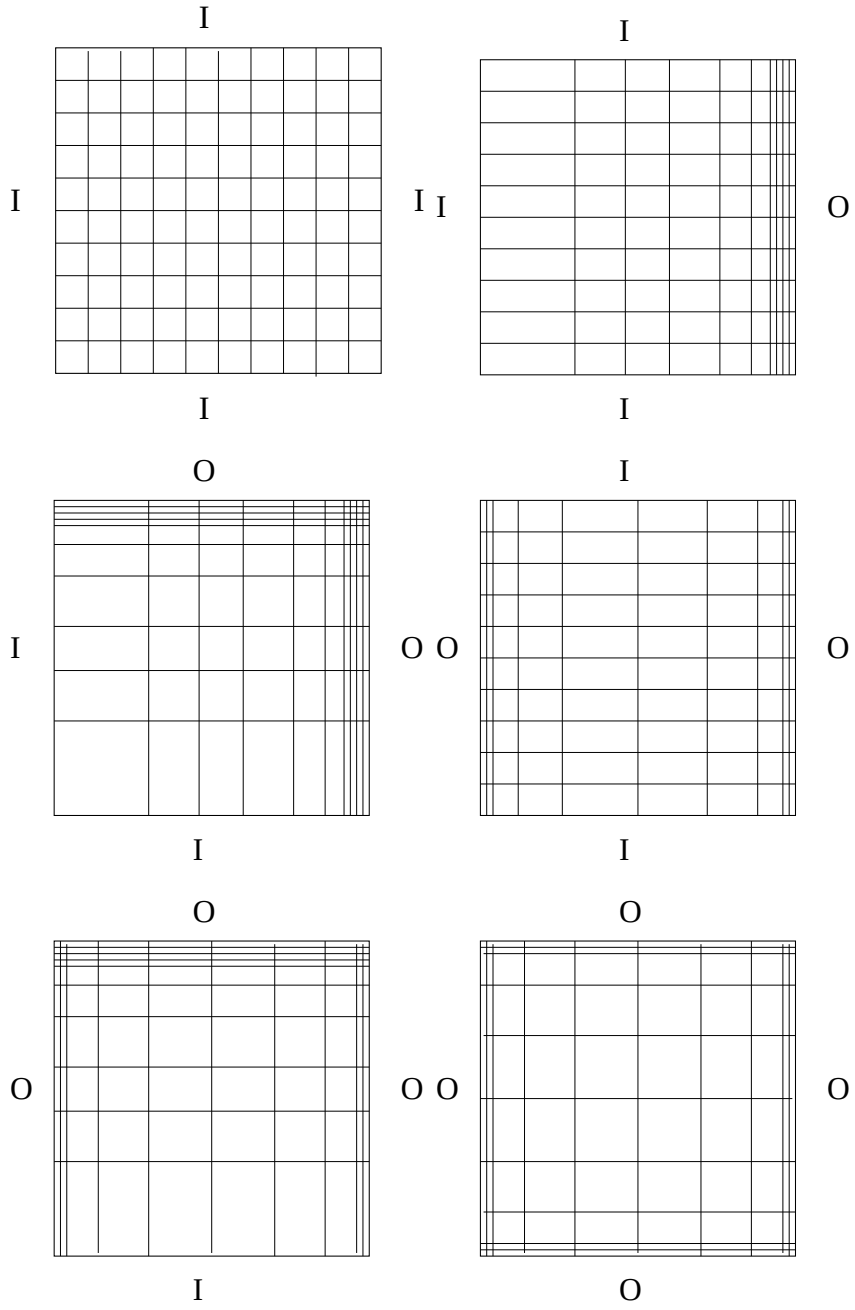

Figure 3.6. Submesh used for different cases: 'I' indicates 'inflow boundary' and 'O' indicates 'outflow' boundary.

4. The algorithm for nonuniform submesh generator

We begin our study of this subject with the algorithm for very simple meshes in one dimension and proceed to generalize to more sophisticated nonuniform irregular mesh generation schemes for the two dimensional case. An algorithm for an uniform mesh on interval (a, b) is easily constructed:

STEP 1 Set $h = \frac{1}{n}$,: n=number of elements

STEP 2 For $i = 1, \cdots, n$:

Set $\alpha_i = (i-1)h$. Then $\bar{\xi}_i = a+(b-a)g_1(\alpha_i)$ defines the node location, where $g_1(\alpha) = \alpha$.

For our nonuniform mesh, we can define two mappings:

$$\xi = g_2(\alpha) = \alpha^2 \tag{4.1}$$

$$\xi = g_3(\alpha) = (1-\alpha)^2. \tag{4.2}$$

Replacing $g_1(\alpha)$ by $g_2(\alpha)$ in the **STEP 2**, the mapping $g_2(\alpha)$ will take the uniform mesh in α to a quadratically graded mesh from left to right in $\bar{\xi}$. (See figure 4.1) Conversely, the mapping $g_3(\alpha)$ will take the uniform mesh in α to a quadratically graded mesh from right to left in $\bar{\xi}$, if we rewrite **STEP 2** as:

For $i = 1, \cdots, n$:

Set $\alpha_i = (i-1)h$. Then $\bar{\xi}_i = b - (b-a)g_3(\alpha_i)$ defined the node location.

Or if we wish to produce a mesh that is graded into both ends $\bar{\xi} = a$ and $\bar{\xi} = b$, we can combine these two mappings $g_2(\alpha)$ and $g_3(\alpha)$ and define

$$g_4(\alpha) = \begin{cases} \alpha^2 & , \quad 0 \le \alpha < 0.5 \\ (1-\alpha)^2 & , \quad 0.5 \le \alpha \le 1 \end{cases} \tag{4.3}$$

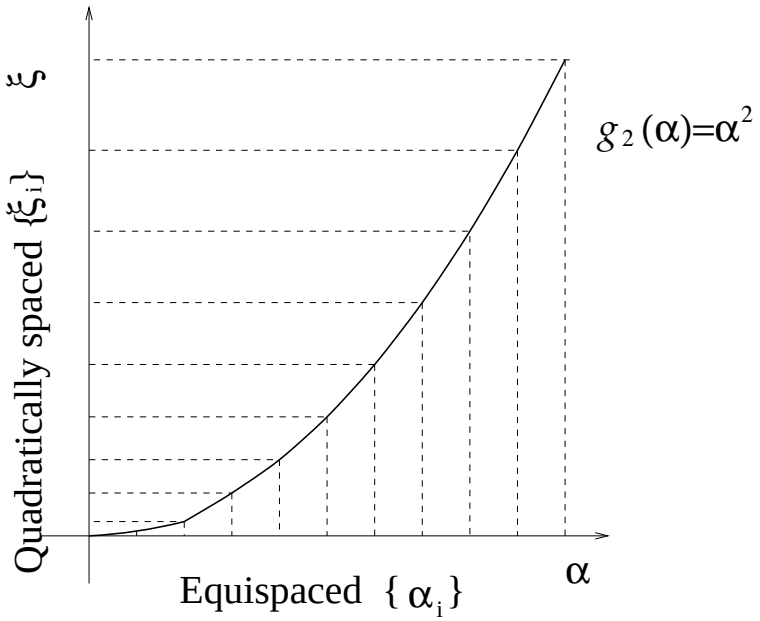

Figure 4.1. Mesh grading from left to right: a quadratic transformation

Now, let us generalize this idea to a two dimensional irregular mesh.

Let K be a quadrilateral element defined by locations of its four nodal points

$x_a^K, a = 1 \cdots, 4$ in the physical domain R^2 and $\Omega^e = [0,1] \times [0,1]$ be a corresponding biunit square in the computational domain. The nodal points and sides of elements either in the physical or the computational domain are labeled in ascending counterclockwise direction. See Figure 4.2.

The coordinates of a point (ξ, η) in the biunit square Ω^e are related to the coordinates of a point (x, y) in K by the transformations:

$$x(\xi, \eta) = \sum_{a=1}^{4} N_a(\xi, \eta) x_a^e \tag{4.4}$$

$$y(\xi, \eta) = \sum_{a=1}^{4} N_a(\xi, \eta) y_a^e, \tag{4.5}$$

$$\text{where } N_1(\xi, \eta) = \frac{1}{4}(1-\xi)(1-\eta), \quad N_2(\xi, \eta) = \frac{1}{4}(1+\xi)(1-\eta),$$
$$N_3(\xi, \eta) = \frac{1}{4}(1+\xi)(1+\eta), \quad N_4(\xi, \eta) = \frac{1}{4}(1-\xi)(1+\eta).$$

Let us introduce some notations used in the algorithm.

1. Nsd: number of space dimensions (Here Nsd=2),
2. N^*es: number of elements for submesh ($N^*es = n \times m$),
3. N^*np: number of nodal points for submesh,
4. a: local node number for mesh ($1 \leq a \leq 4$)
5. a^*: local node number for submesh ($1 \leq a^* \leq 4$),
6. A^* global node number for submesh ($1 \leq A^* \leq N^*np$),

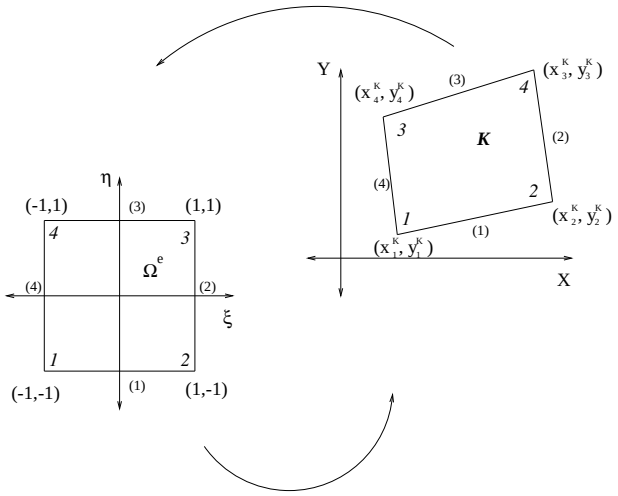

Figure 4.2. Local node and side ordering

7. i: spatial index ($1 \leq i \leq Nsd$),

8. e^* : element number for submesh ($1 \leq i^* \leq N^*es$),

9. ID$^*(A^*)$: destination matrix for submesh.

10. IEN$^*(a^*, e^*)$: location matrix for submesh.

11. $x^K(a, i)$: coordinates of nodal points for mesh

12. $x^{K^*}(A^*, i)$ coordinates of global node number for submesh

Similarly to the global level, three data processing arrays, IEN*, ID* and $x^{K^*}(A^*, i^*)$ are needed as input data. For more detailed discussion see [9].

Here is the algorithm for the irregular mesh generator:

INPUT: $x^K(a, i)$, m, n

OUTPUT: ID*(A*), LM*(a*,e*), $x^{K^*}(A^*, i)$

STEP 1 Determine whether each boundary of element K is 'inflow 'or 'outflow' by the definition and then properly label each corresponding segment of the biunit square Ω^e.

STEP 2 Set $h = \frac{2}{n}$, $k = \frac{2}{m}$.

STEP 3 Compute the horizontal coordinates of the submesh for the biunit square Ω^e:

Define the following mapping:

$$f_1(x) = x^3 \tag{4.6}$$

$$f_2(x) = (1-x)^3 \tag{4.7}$$

$$f_3(x) = x \tag{4.8}$$

Note: The domains of these three functions are [0,1].

Case 1: Side(2) and Side(4) both are 'inflow' boundary segments

For $i = 1, \cdots, n+1$:

Set $\alpha_i = (i-1)h$. Then $\bar{\xi}_i = -1 + 2f_3(\alpha_i)$;

Case 2: Side(2) and Side(4) both are 'outflow' boundary segments

For $i = 1, \cdots, [n/2]$:

Set $\alpha_i = (i-1)h$. Then $\bar{\xi}_i = -1 + 2f_1(\alpha_i)$ and

for $i = [n/2+1], \cdots, n+1$:

Set $\alpha_i = (i-1)h$. Then $\bar{\xi}_i = 1 - 2f_2(\alpha_i)$;

Case 3: Side(2) is 'inflow' and Side(4) is 'outflow' boundary segment

For $i = 1, \cdots, n$:

Set $\alpha_i = (i-1)h$. Then $\bar{\xi}_i = -1 + 2f_1(\alpha_i)$;

Case 4: Side(2) is 'outflow' and side(4) is 'inflow' boundary segment

For $i = 1, \cdots, n$:

Set $\alpha_i = (i-1)h$. Then $\bar{\xi}_i = 1 - 2f_2(\alpha_i)$;

STEP 4 Compute the vertical coordinates of the submesh for biunit square Ω^e.

Similar to **STEP 3**, now we consider Side(1) and Side(3) of Ω^e.

STEP 5 Set ID$^*(A^*)$=0 on the boundary nodes and eq=1;

STEP 6 For $i = 1, \cdots, n$; $j = 1, \ldots, m$: do **STEP 7 - STEP 10**

STEP 7 Construct ID$^*(A^*)$ for submesh

Set $A^* = (i-1) * (n+1) + j$, $A^* \equiv (i, j)$;

If ID$^*(A^*) \neq 0$ then ID(A^*)=eq and set eq=eq+1;

STEP 8 Construct IEN$^*(a^*, e^*)$ for submesh:

Set $e^* = (i-1) * (n+1) + j$;

Then IEN*(1,e^*)=A^*, IEN*(2,e^*)=A^*+1,

IEN*(3,e^*)=A^* + n+2, IEN*(4,e^*)=A^* + n+1.

STEP 9 Compute the coordinate of node points (node A^*):

$$\begin{aligned} \xi_{A^*} &= \bar{\xi}_i \\ \eta_{A^*} &= \bar{\eta}_j \end{aligned} \tag{4.9}$$

STEP 10 Map the coordinates of node points (ξ_{A^*}, η_{A^*}) from the computational domain to the physical domain by the transformations (4.4) and (4.5).

5. Numerical results

In this chapter, we will report three series of experiments for the advection-diffusion problem with TLFEM using the new non-uniform submesh introduced in the previous section. In the following numerical results, we illustrate the applicability of the method for singularly perturbed problems, i.e. for small values of the diffusivity κ compared with the advection field .

5.1 A problem with discontinuous boundary condition

In the first two experiments, let us consider a unit square domain Ω with discontinuous boundary values at (0.5,0) and (0,1). The diffusivity is $\kappa = 10^{-6}$, and we will test our methods for two different angles of the uniform velocity field of size one with the horizontal axis. The first case is 45^o and the second one is 60^o. (see Figure 5.1 for problem statements).

In these problems, a discontinuous data at the inflow boundary is propagated into the domain which causes an internal layer along the characteristic of the problem starting at point(0.5,0). In addition, the problems are subjected to homogeneous Dirichlet boundary conditions at the outflow boundary which create the outflow boundaries.

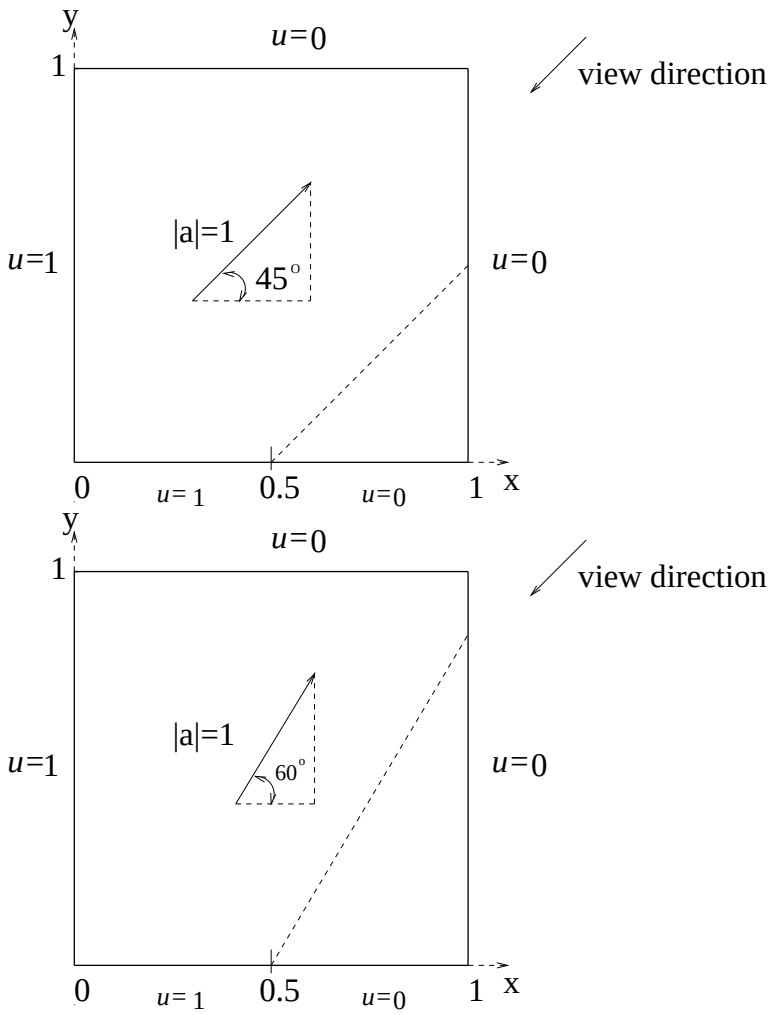

Figure 5.1. Domain for skew convection problems with two different velocity fields

For both cases, we employ an $20\times$ 20 uniform mesh for the TLFEM and the GLS methods. First, we compare the different submesh partition strategies for the TLFEM, say 10×10 uniform submesh and nonuniform submesh(See Figure 5.2) For bubble shape function analysis, we pick one element to plot

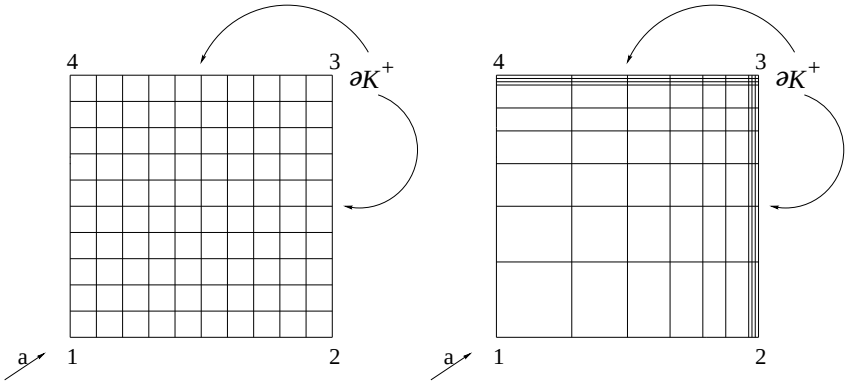

Figure 5.2. Two different 10x10 submeshes used for TLFEM: uniform (left) and nonuniform (right).

four shape bubble functions. The comparison of bubble shape functions by using uniform and nonuniform submesh for 45^o case is shown in Figure 5.3, and for 60^o is shown in Figure 5.4. For both cases, it is obvious that nonuniform submeshes are successful to capture the outflow boundary layers, and produce more accurate residual free shape functions. Meanwhile, the nonuniform submesh yields slightly better performance in the global solutions for both cases. (see Figure 5.5 and 5.6.) In Figure 5.7 and Figure 5.8, both the TLFEM and the GLS perform similarly except in the crosswind internal boundary layer. TLFEM performs better than GLS therein.

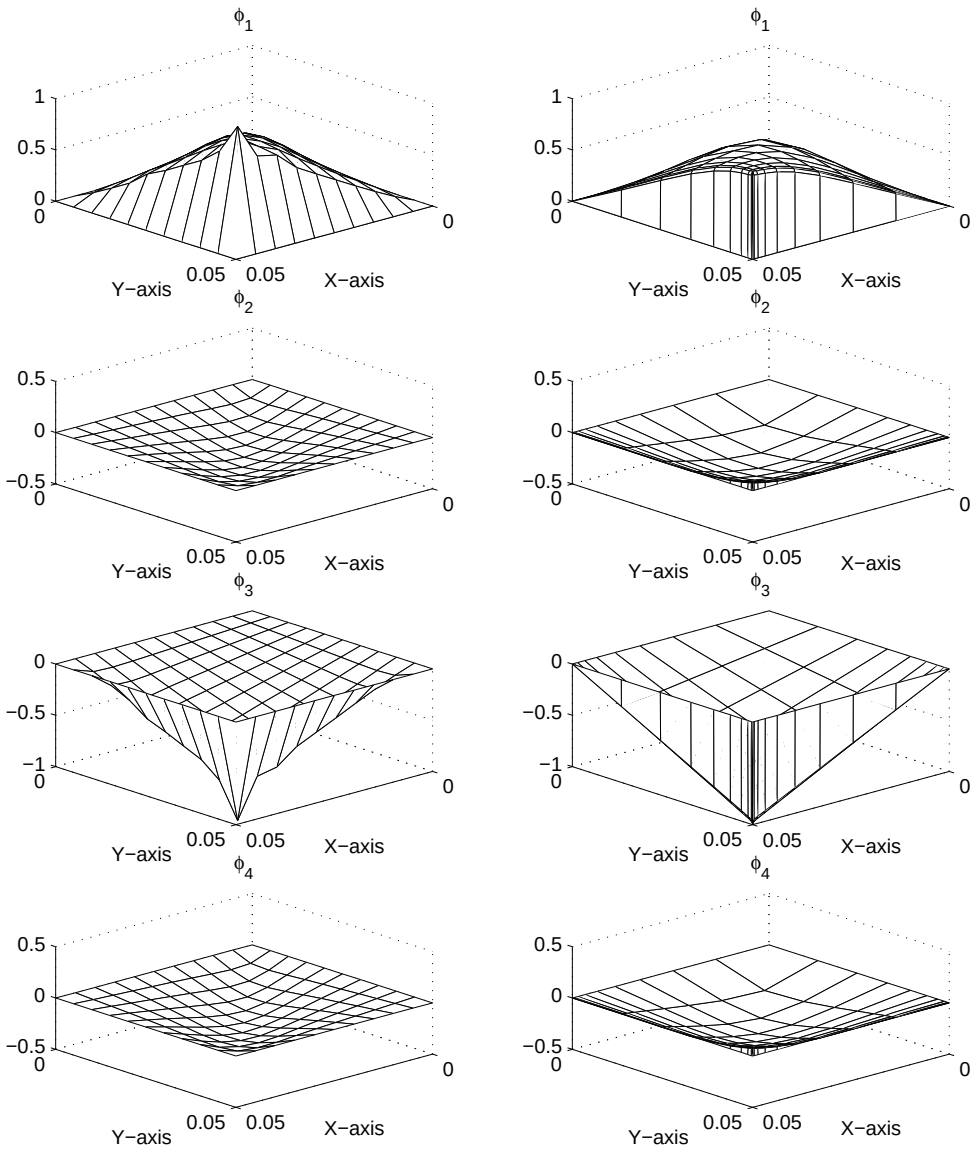

Figure 5.3. Comparison of bubble shape functions by using two different submeshes for the 45^o problem: uniform (left) and nonuniform (right)

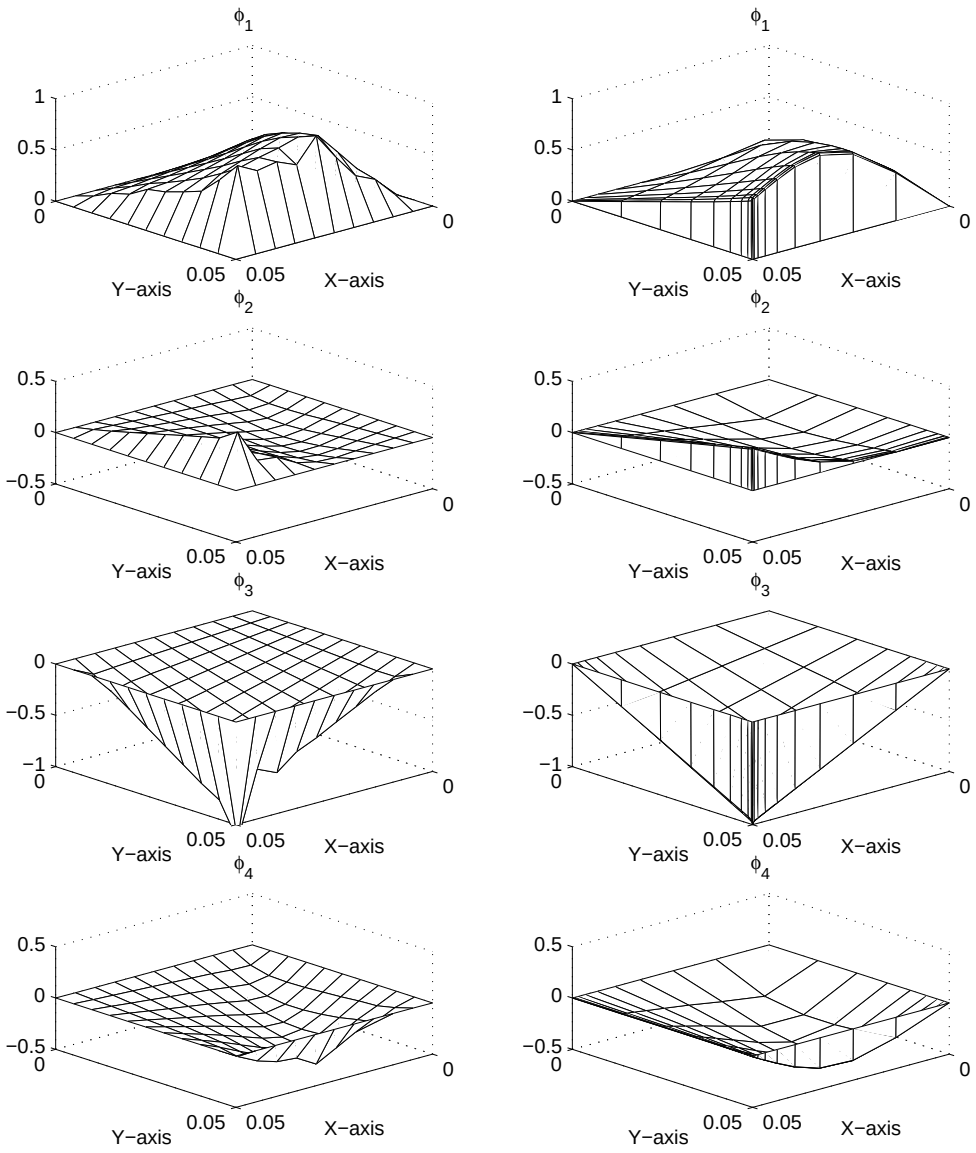

Figure 5.4. Comparison of bubble shape functions by using two different submeshes for the 60^o problem: uniform (left) and nonuniform (right)

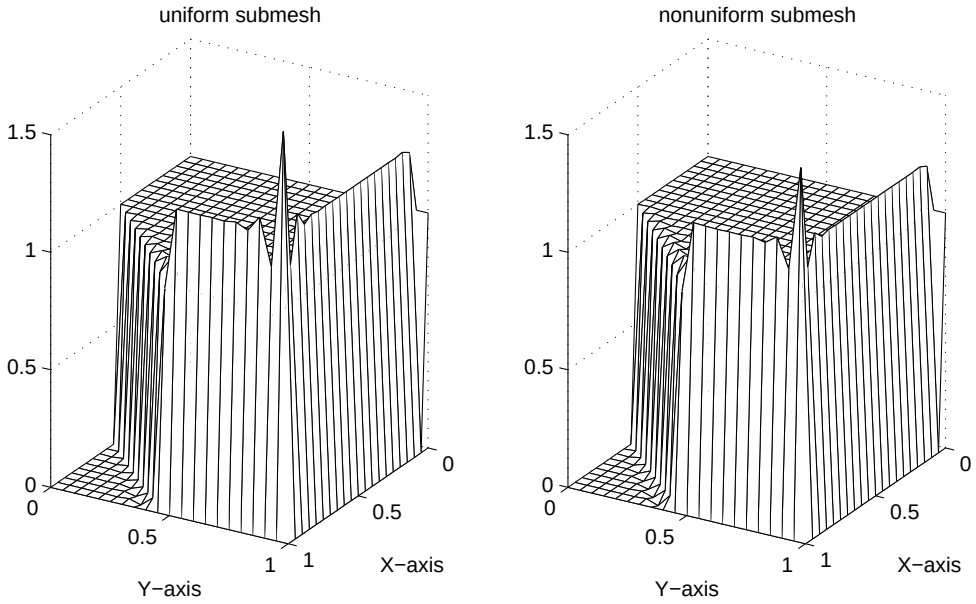

Figure 5.5. Comparison of TLFEM solutions by using two different submeshes for the 45^o problem: uniform (left) and nonuniform (right)

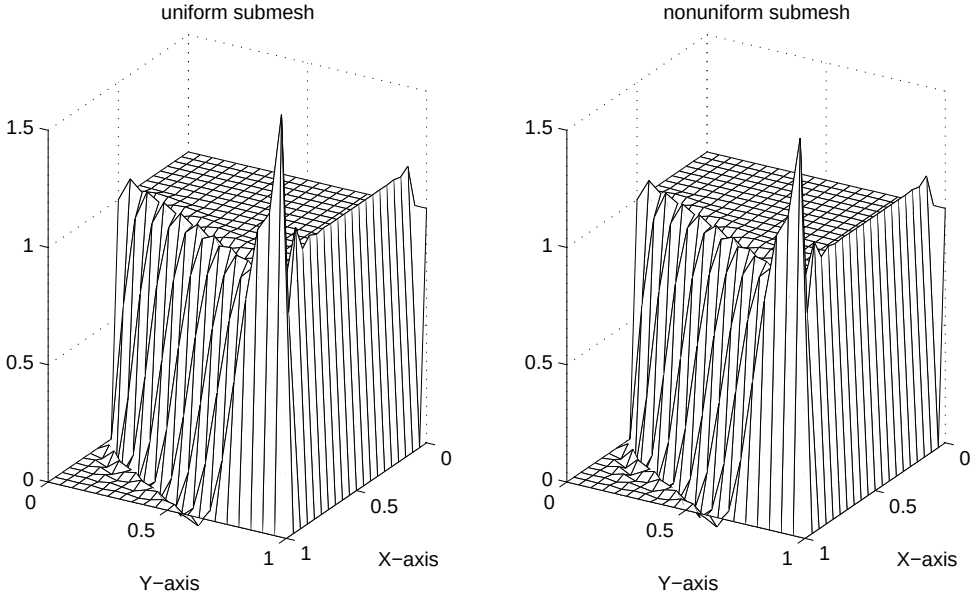

Figure 5.6. Comparison of TLFEM solutions by using two different submeshes for the 60^o problem: uniform (left) and nonuniform (right)

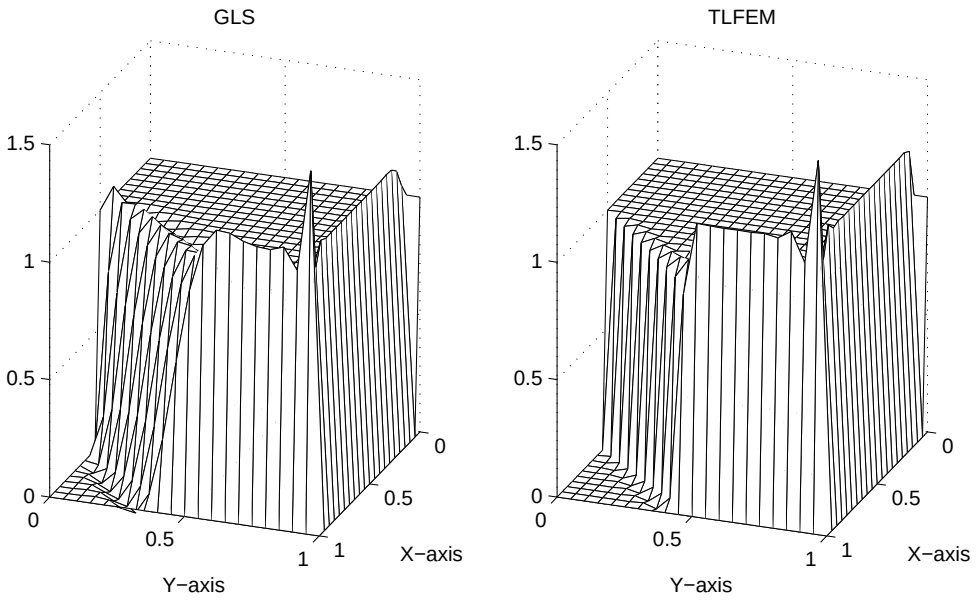

Figure 5.7. Comparison of GLS and TLFEM solutions for the 45^o problem: GLS (left) and TLFEM (right)

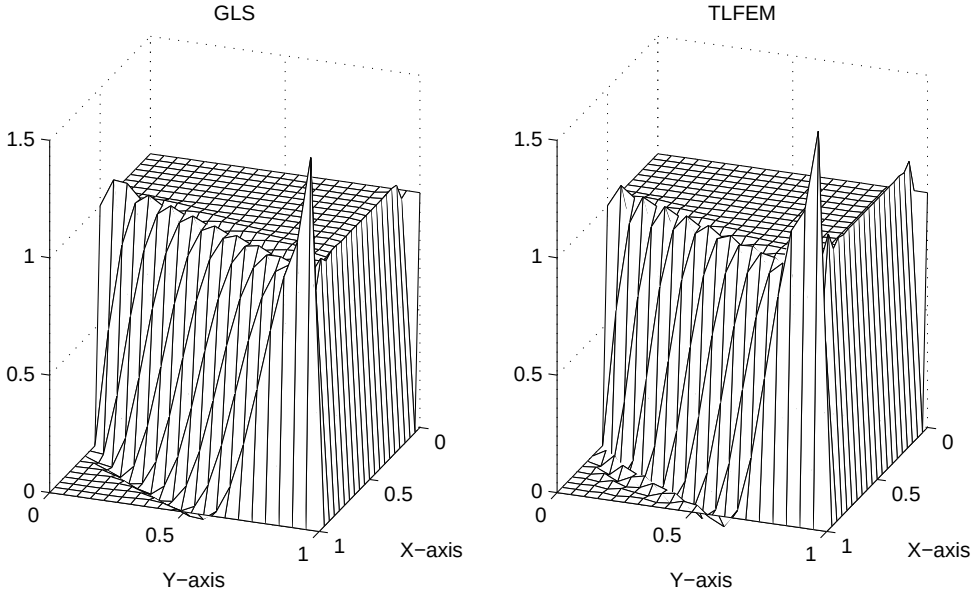

Figure 5.8. Comparison of GLS and TLFEM solutions for the 60^o problem: GLS (left) and TLFEM (right)

5.2 Thermal boundary layer problem

Let us consider a rectangular domain of sides 1.0 and 0.5. subject to the boundary conditions presented in Figure 5.9. The velocity field is given by $a = (2y, 0)$ and diffusivity $\kappa = 7 \times 10^{-4}$. This problem can be viewed as the simulation of the development of a thermal boundary layer on a fully developed flow between two parallel plates, where the top plate is moving with the velocity equal to one and the bottom plate is fixed.

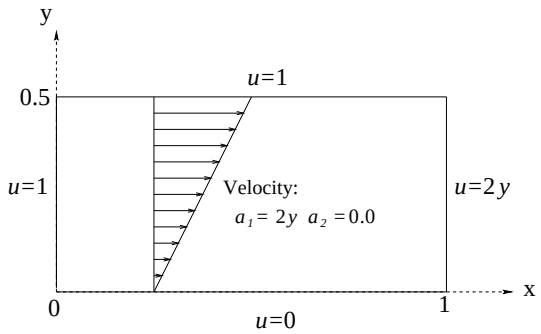

Figure 5.9. Problem statement for the thermal boundary layer problem

The non-homogeneous mesh for GLS and TLFEM methods consists 21 equally spaced nodes in the x-direction, 11 nodes uniformly distributed in the interval [0,0.1] and 11 nodes equally spaced on [0.1,0.5] in the y-direction. (see Figure 5.10)

We wish to compare TLFEM by using the different submeshes, say 10×10 uniform and nonuniform submesh (see Figure 5.11).

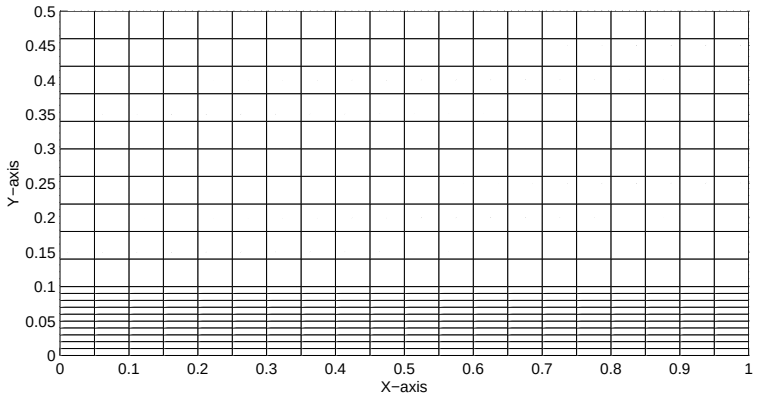

Figure 5.10. Mesh used for the thermal boundary layer problem

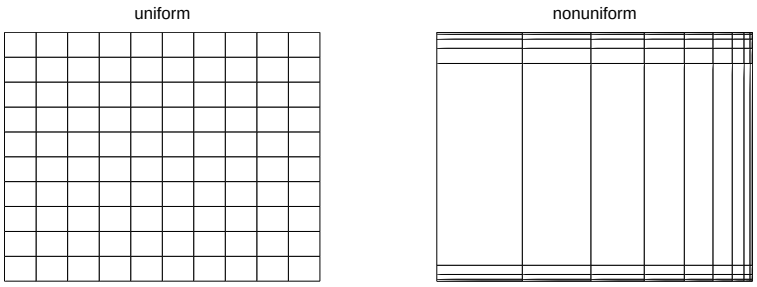

Figure 5.11. Submesh used for the thermal boundary layer problem

Because the flow velocity increases along the y-direction, the characteristics of solutions in the domain can be divided into two regions: for the bottom of the domain, we have a diffusive dominated case ; for the top of the domain, we have the advective dominated case.

We find out that the uniform submesh performs better than the nonuniform mesh for the diffusive dominated case. On the other hand, the nonuniform submesh still does a good job for the advective dominated case (See Figures 5.13 and 5.14). The global solutions for the two different submeshes are almost the same (See Figure 5.12).

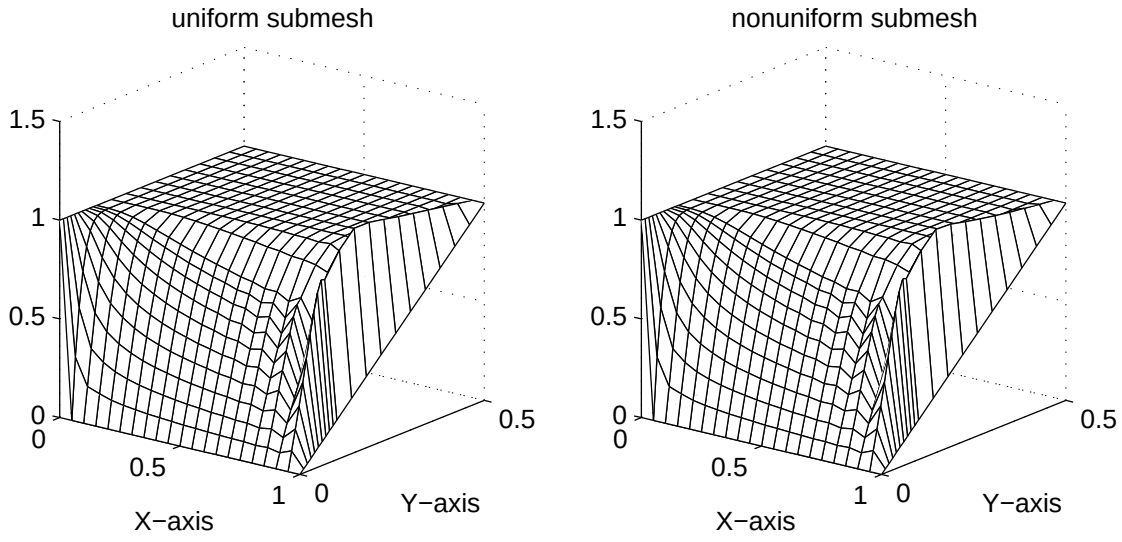

Figure 5.12. Comparison of TLFEM solutions using two different submeshes

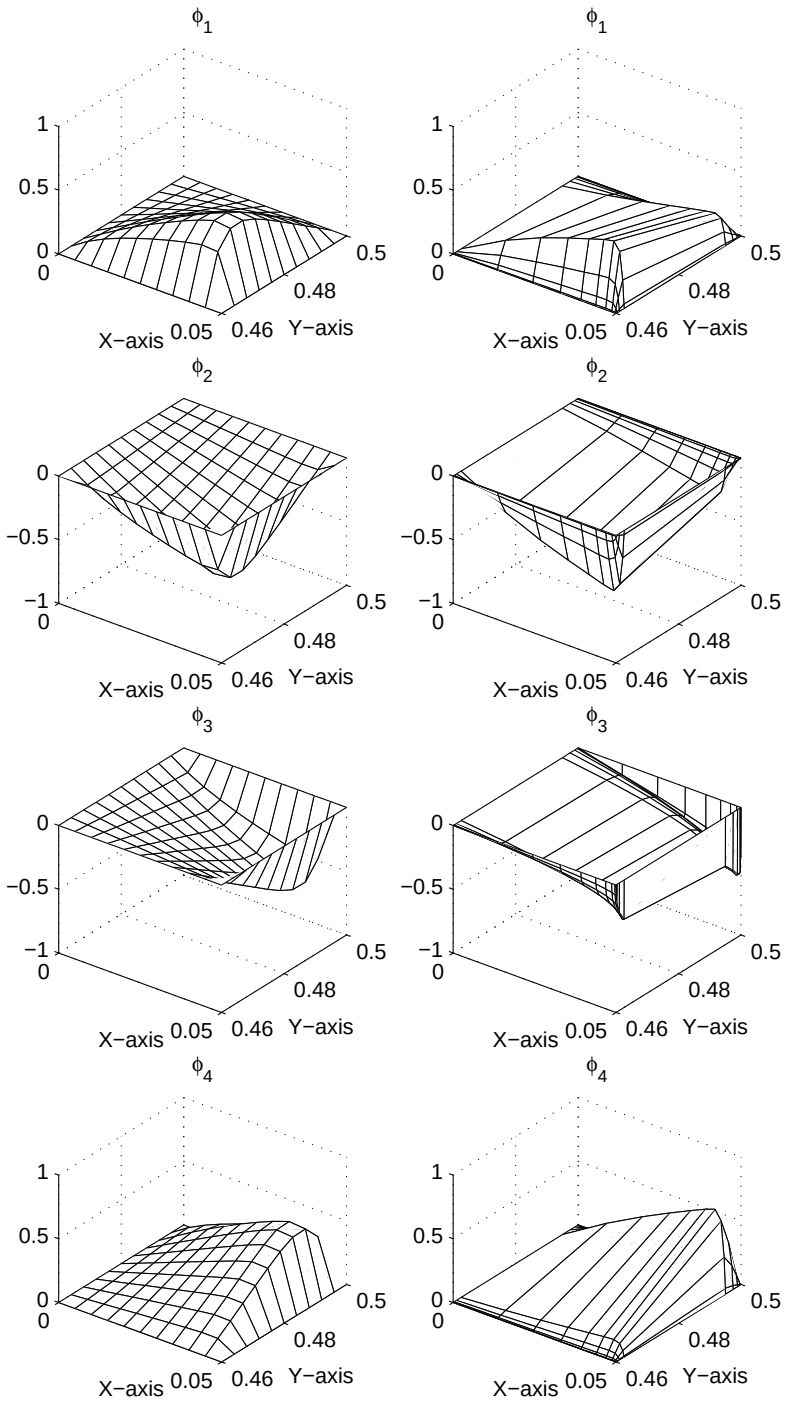

Figure 5.13. Bubble shape functions for the diffusive dominated case: uniform submesh (left) and nonuniform submesh (right)

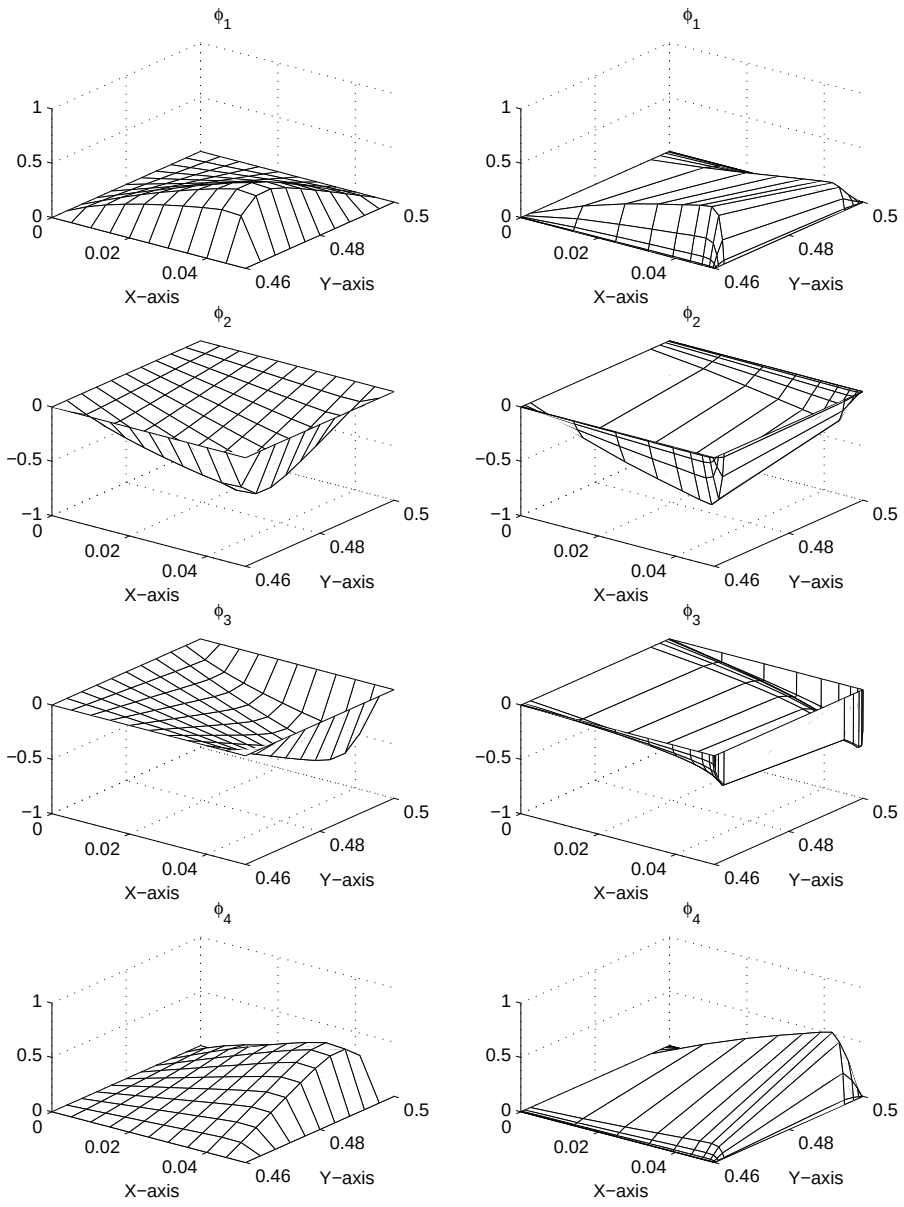

Figure 5.14. Bubble shape functions for the advective dominated case: uniform submesh (left) and nonuniform submesh (right)

Next we change to a smaller diffusivity $\kappa = 10^{-6}$ and rerun TLFEM by using the same meshes and submeshes and compare it with the GLS method (See Figures 5.15 and 5.16 for the bubble shape functions comparison). Taking the top plate velocity as the characteristic flow velocity, we have the mesh-Peclet number $Pe = \dfrac{|\boldsymbol{a}|h}{2\kappa} = 25000$. This means that the entire domain is advectively dominated. The numerical results show that the nonuniform submesh performs slightly better than the uniform one (See Figure 5.17). Meanwhile, the TLFEM performs better than the GLS (See Figure 5.18). There are some oscillations near the outflow boundary.

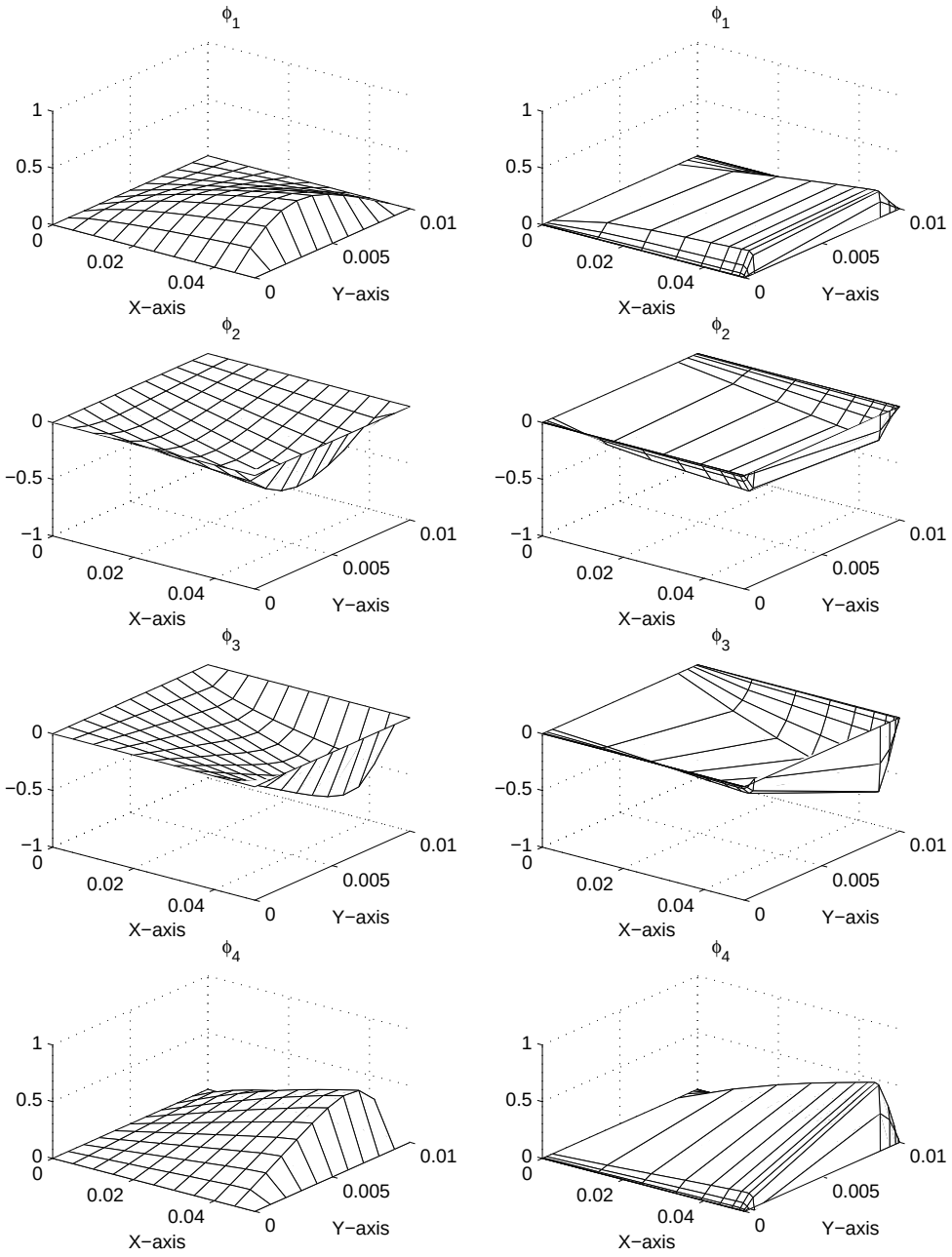

Figure 5.15. Bubble shape functions approximated by two different submeshes for the bottom region: uniform (left) and nonuniform (right)

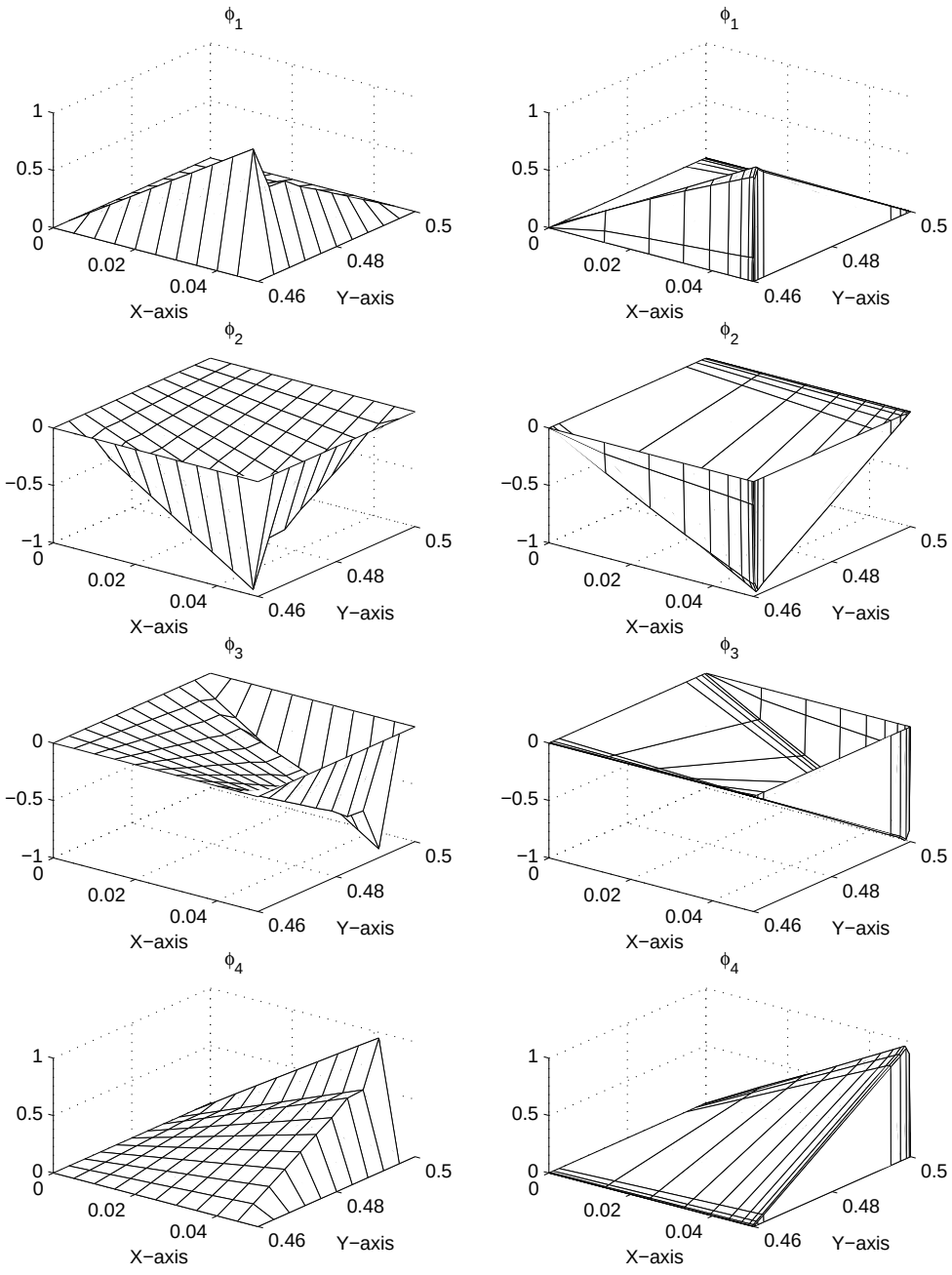

Figure 5.16. Bubble shape functions approximated by two different submeshes for the top region: uniform (left) and nonuniform (right)

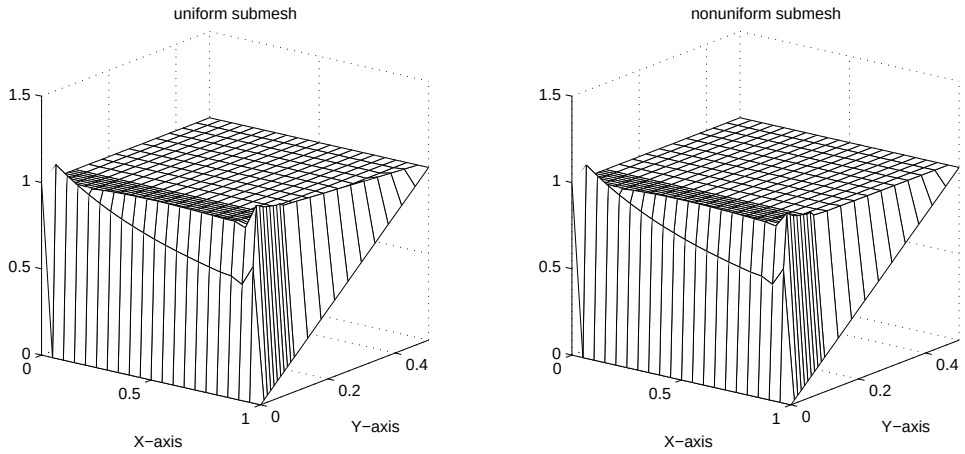

Figure 5.17. Comparison of the TLFEM solutions by using two different submeshes for the thermal boundary layer problem when $\kappa = 10^{-6}$: uniform (left) and nonuniform (right)

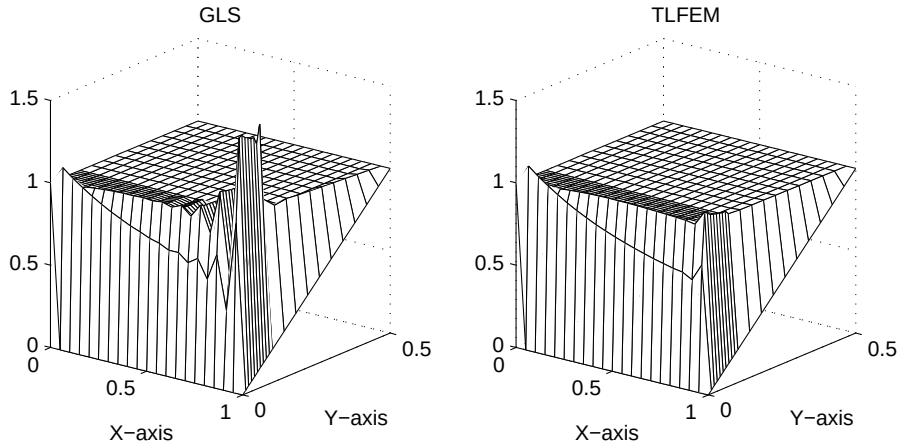

Figure 5.18. Comparison between the GLS method and the TLFEM method for the thermal boundary layer problem when $\kappa = 10^{-6}$: GLS (left) and TLFEM (right)

5.3 Bubble ramp problem

Now, let us consider an L-shaped domain with external source f=1, $\kappa = 10^{-6}$, and homogeneous Dirichlet conditions depicted in Figure 5.16

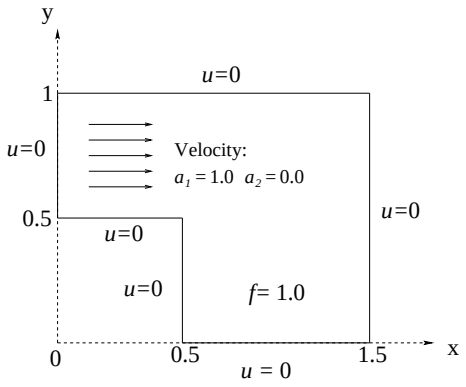

Figure 5.19. Problem statement for the bubble ramp problem

A uniform partition into 300 elements are employed for the global mesh and two kinds of 10×10 submeshes are used for TLFEM. Because of the presence of the external force, the additional residual free bubble shape function ϕ_f needs to be determined. The comparison of these approximated solutions using two different submeshes are shown in Figure 5.20, where the nonuniform submesh performs better than the uniform one.

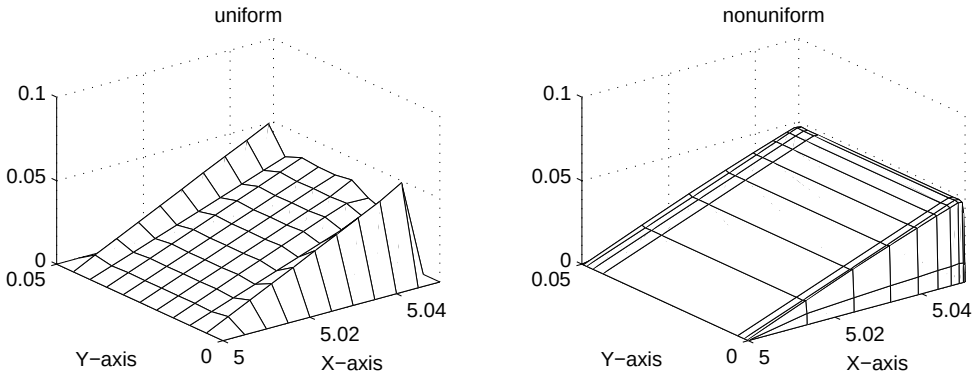

Figure 5.20. Comparison of bubble shape function ϕ_f by using two different submesh for the bubble ramp problem: uniform(left) and nonuniform (right)

The solution exhibits a strong outflow boundary layer along x=1.5, two crosswind boundary layers along y=1 and y=0, and a crosswind internal layer along y=0.5. Thus, it is one of the most stringent tests for the advective diffusive problem. We find out that there are some improvements near outflow boundaries in the numerical solutions for the TLFEM due to the new submesh we choose. Meanwhile, the numerical results of the GLS and the TLFEM using nonuniform submeshes are almost indistinguishable (See Figure 5.21).

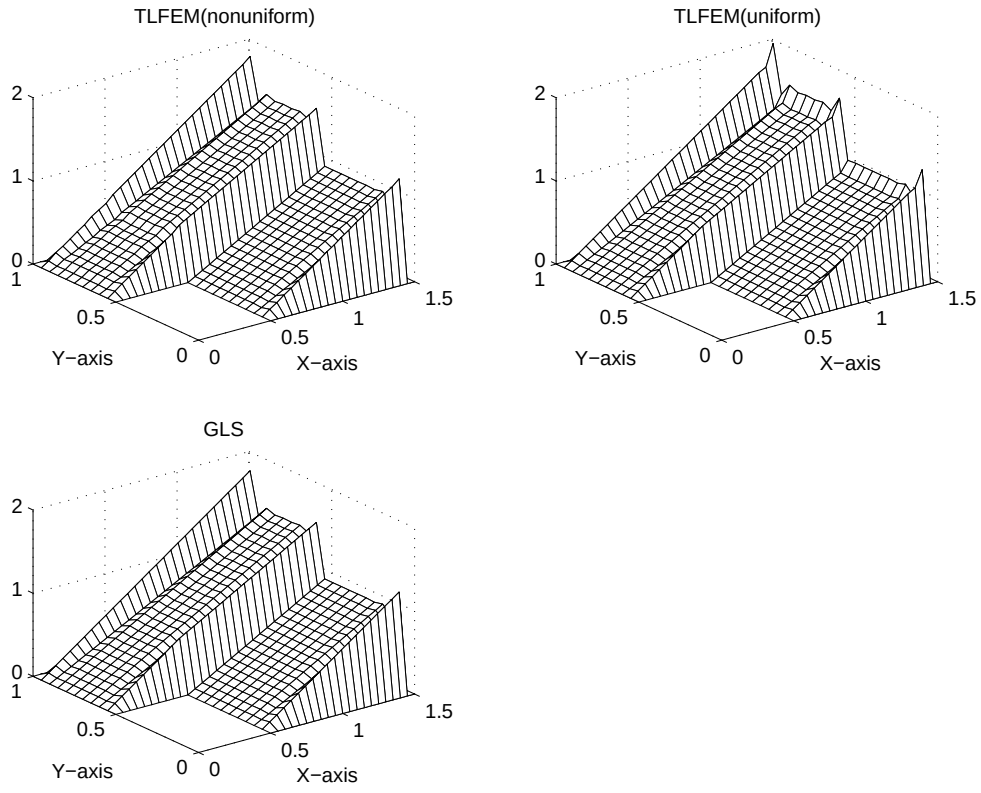

Figure 5.21. Comparison of the GLS and the TLFEM by using two different submeshes for the bubble ramp problem

6. Conclusion

In this work, we formulated the two-level finite element method based on the standard Galerkin method using piecewise linears in the original mesh, and the usual stabilized finite element method was used to approximate the partial differential equations governing the residual free bubble functions. Once these residual free bubble functions are determined, we can substitute them into the Galerkin formulation to improve the accuracy of the global numerical solution. The main advantage of this method is that we do not have to solve these partial differential equations analytically. Therefore, it is suitable for the finite element computation in a practical problem.

Due to the choice of bubble functions, the boundary layers occur at outflow boundaries for the advective-dominated case. The new submesh strategy was introduced to cure this problem. The numerical experiments confirm our idea that non-uniform submeshes are able to capture the layer of residual free bubble shape functions. The result display some improvements in the solution of the advective-diffusive problem, and the TLFEM solutions perform better than the GLS method in some cases. We note that the idea of the new submesh strategy can be applied to other problems in fluid dynamics,

such as the incompressible Naiver-Stokes equations. Non-uniform submesh depending on the direction of the flow can approximate the solution of the pressure term more accurately. See [12] for its application.

References

[1] F. Brezzi, M.O. Bristeau, L.P. Franca, M. Mallet, and G. Roge. A relationship between stabilized finite element methods and the Galerkin method with bubble functions. *Comput. Methods Appl. Mech. Engrg.*, 96: 117-129, 1992.

[2] F. Brezzi, L.P. Franca, A. Russo. Further considerations on residual-free bubbles for advective-diffusive equations. *Methods Appl. Mech. Engrg.*, 166: 25-33, 1998.

[3] A.N. Brooks and T.J.R. Hughes. Streamline upwind/Petrov-Galerkin formulation for convection dominated flows with particular emphasis on the imcompressible Navier-Stokes equations. *Comput. Methods. Appl. Mech. Engrg.*, 32: 199-259, 1982.

[4] G.F. Carey and J.T. Oden. *Finite Elements: Computational aspects.* Prentice-Hall, 1984.

[5] L.P. Franca, S.L Frey and T.J.R. Hughes. Stabilized finite element methods: I. Application to advective-diffusive model. *Comput. Methods. Appl. Engrg.*, 95: 253-276, 1992.

[6] L.P. Franca and A.P. Macedo, A two-level finite element method and its application to Helmholtz equation. *Int. J. Numer. Methods Engrg.*, 43: 23-32, 1998.

[7] L. P. Franca, A. Nesliturk, and M. Stynes. On the satibility of residual-free bubbles for convection-diffusion problems and their approximation by a two-level finite element method. *Comput. Methods Appl. Mech. Engrg.*, 166: 35-49, 1998.

[8] L. P. Franca and F. Valentin. On an improved ususual stabilized finite element method for the advective-reactive-diffusive equation, To appear

[9] T.J.R. Hughes. *The Finite Element Method: Linear Static and Dynamic Finite Element Analysis.* Prentice-Hall, 1987.

[10] T.J.R. Hughes, L.P. Franca, and G.M. Hulbert, A new finite element

formulation for computational fluid dynamics: VIII. The Galerkin/least-squares method for advective-diffusive equations *Comput.Methods Appl. Mech. Engrg.,* 73: 173-189, 1989.

[11] C. Johnson. *Numerical Solution of Partial Differential Equations by the Finite Element Method.* Cambridge, 1987.

[12] A. Nesliturk. *Approximating the incompressible Navier Stokes equations by the two-level finite element method.* Ph.D thesis, University of Colorado at Denver, 1999.